We are IntechOpen,
the world's leading publisher of
Open Access books
Built by scientists, for scientists

6,900
Open access books available

185,000
International authors and editors

200M
Downloads

154
Countries delivered to

Our authors are among the

TOP 1%
most cited scientists

12.2%
Contributors from top 500 universities

BOOK CITATION INDEX
CLARIVATE ANALYTICS
INDEXED

WEB OF SCIENCE™

Selection of our books indexed in the Book Citation Index
in Web of Science™ Core Collection (BKCI)

Interested in publishing with us?
Contact book.department@intechopen.com

Numbers displayed above are based on latest data collected.
For more information visit www.intechopen.com

Atmospheric Refraction and Propagation in Lower Troposphere

Martin Grabner and Vaclav Kvicera
Czech Metrology Institute
Czech Republic

1. Introduction

Influence of atmospheric refraction on the propagation of electromagnetic waves has been studied from the beginnings of radio wave technology (Kerr, 1987). It has been proved that the path bending of electromagnetic waves due to inhomogeneous spatial distribution of the refractive index of air causes adverse effects such as multipath fading and interference, attenuation due to diffraction on the terrain obstacles or so called radio holes (Lavergnat & Sylvain, 2000). These effects significantly impair radio communication, navigation and radar systems. Atmospheric refractivity is dependent on physical parameters of air such as pressure, temperature and water content. It varies in space and time due the physical processes in atmosphere that are often difficult to describe in a deterministic way and have to be, to some extent, considered as random with its probabilistic characteristics.

Current research of refractivity effects utilizes both the experimental results obtained from in situ measurements of atmospheric refractivity and the computational methods to simulate the refractivity related propagation effects. The two following areas are mainly addressed. First, a more complete statistical description of refractivity distribution is sought using the finer space and time scales in order to get data not only for typical current applications such as radio path planning, but also to describe adverse propagation in detail. For example, multipath propagation can be caused by atmospheric layers of width of several meters. During severe multipath propagation conditions, received signal changes on time scales of minutes or seconds. Therefore, for example, the vertical profiles of meteorological parameters measured every 6 hours by radiosondes are not sufficient for all modelling purposes. The second main topic of an ongoing research is a development and application of inverse propagation methods that are intended to obtain refractivity fields from electromagnetic measurements.

In the chapter, recent experimental and modelling results are presented that are related to atmospheric refractivity effects on the propagation of microwaves in the lowest troposphere. The chapter is organized as follows. Basic facts about atmospheric refractivity are introduced in the Section 2. The current experimental measurement of the vertical distribution of refractivity is described in the Section 3. Long term statistics of atmospheric refractivity parameters are presented in the Section 4. Finally, the methods of propagation modelling of EM waves in the lowest troposphere with inhomogeneous refractivity are discussed in the Section 5.

2. Atmospheric refractivity

2.1 Physical parameters of air and refractivity formula

The refractive index of air n is related to the dielectric constants of the gas constituents of an air mixture. Its numerical value is only slightly larger than one. Therefore, a more convenient atmospheric refractivity N (N-units) is usually introduced as:

$$N = (n-1) \times 10^6 \tag{1}$$

It can be simply demonstrated, based on the Debye theory of polar molecules, that refractivity can be calculated from pressure p (hPa) and temperature T (K) as (Brussaard, 1996):

$$N = \frac{77.6}{T}\left(p + 4810\frac{e}{T} \right) \tag{2}$$

where e (hPa) stands for a water vapour pressure that is related to the relative humidity H (%) by a relation:

$$H = 100\, e/e_s(t) \tag{3}$$

where e_s (hPa) is a saturation vapour pressure. The saturation pressure e_s depends on temperature t (°C) according to the following empirical equation:

$$e_s(t) = a\exp\big(bt/(t+c)\big) \tag{4}$$

where for the saturation vapour above liquid water $a = 6.1121$ hPa, $b = 17.502$ and $c = 240.97$ °C and above ice $a = 6.1115$ hPa, $b = 22.452$ and $c = 272.55$ °C.

It is seen in Fig.1a where the dependence of the refractivity on temperature and relative humidity is depicted that refractivity generally increases with humidity. Its dependence on temperature is not generally monotonic however. For humidity values larger than about 40%, refractivity also increases with temperature.
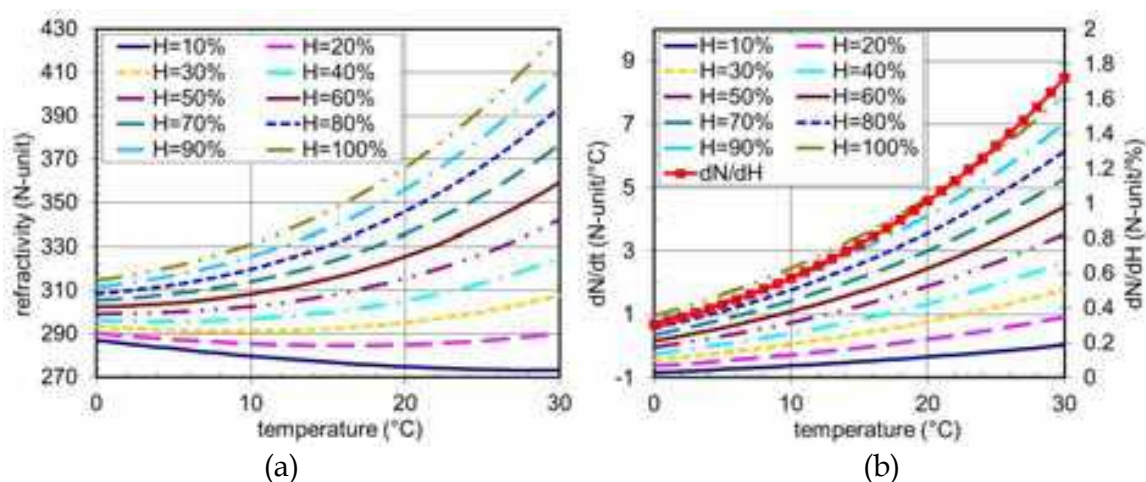

Fig. 1. The radio refractivity dependence on temperature and relative humidity of air for pressure $p = 1000$ hPa (a), refractivity sensitivity dependence on temperature and relative humidity of air (b).

The *sensitivity* of refractivity on temperature and relative humidity of air is shown in Fig. 1b. For t = 10°C (cca average near ground temperature in the Czech Republic), H = 70% (cca average near ground relative humidity) and p = 1000 hPa, the sensitivities are dN/dt = 1.43 N-unit/°C, dN/dH = 0.57 N-unit/% and dN/dp = 0.27 N-unit/hPa. The refractivity variation is usually most significantly influenced by the changes of relative humidity as a water vapour content often changes rapidly (both in space and time) and it is least sensitive to pressure variation. However a decrease in pressure with altitude is mainly responsible for a standard vertical gradient of the atmospheric refractivity.

During standard atmospheric conditions, the temperature and pressure are decreasing with the height above the ground with lapse rates of about 6 °C/km and 125 hPa/km (near ground gradients). Assuming that relative humidity is approximately constant with height, a standard value of the lapse rate of refractivity with a height h can be obtained using pressure and temperature sensitivities and their standard lapse rates. Such an estimated standard vertical gradient of refractivity is about $dN/dh \approx$ -42 N-units/km. It will be seen that such value is very close to the observed long term median of the vertical gradient of refractivity.

2.2 EM wave propagation basics

Ray approximation of EM wave propagation is convenient to see the basic propagation characteristics in real atmosphere. The ray equation can be written in a vector form as:

$$\frac{d}{ds}\left(n\frac{d\mathbf{r}}{ds} \right) = \nabla n \tag{5}$$

where a position vector $\mathbf{r}$ is associated with each point along a ray and s is the curvilinear abscissa along this ray. Since the atmosphere is dominantly *horizontally stratified*, the gradient ∇n has its main component in vertical direction. Considering nearly horizontal propagation, the refractive index close to one and only vertical component of the gradient ∇n, one can derive from (5) that the *inverse* of the radius of ray curvature, ρ, is approximately equal to the negative height derivative of the refractive index, $-dn/dh$. Using the conservation of a relative curvature: $1/R$ - $1/\rho$ = const. = $1/R_{ef}$ - $1/\infty$ one can transform the curvilinear ray to a straight line propagating above an Earth surface with the effective Earth radius R_{ef} given by:

$$R_{ef} = R\left/ \left(1 - \frac{R}{\rho} \right) \right. = R\left/ \left(1 + R\frac{dN}{dh}10^{-6} \right) \right. \tag{6}$$

where R stands for the Earth radius and dN/dh denotes a vertical gradient of refractivity.

Three typical propagation conditions are observed depending on the numerical value of the gradient. If $dN/dh \approx$ -40 N-units/km, than from (6): $R_{ef} \approx 4/3\ R$ and standard atmospheric conditions take place. The standard value of the vertical refractivity gradient is approximately equal to the long term median of the gradient observed in mild climate areas. The median gradients observed in other climate regions may be slightly different, see the world maps of refractivity statistics in (Rec. ITU-R P.453-9, 2009).

Sub-refractive atmospheric conditions occur when the refractivity gradient has a significantly larger value, super-refractive conditions occur when the refractivity gradient is well below the standard value of -40 N-units/km. During sub-refractive atmospheric conditions, the effective

Earth radius R_{ef} decreases, terrain obstacles are relatively higher and the received signal may by attenuated due to diffraction loss appearing if the obstacle interfere more than 60% of the radius of the 1st Fresnel ellipsoid on the line between the transmitter and receiver. During super-refractive conditions, on the other hand, the effective Earth radius is lower than the Earth radius R or it is even negative when dN/dh < -157 N-units/km. It means a radio path is more "open" in the sense that terrain obstacles are relatively lower. Super-refractive conditions are often associated with multipath propagation when the received signal fluctuates due to constructive and destructive interference of EM waves coming to the receiver antenna with different phase shifts or time delays.

In principle, the EM wave propagation characteristics during clear-air conditions are straightforwardly determined by the state of atmospheric refractivity. Nevertheless, atmospheric refractivity varies in time and space more or less randomly and full details of it are out of reach in practice. Therefore the *statistics* of atmospheric refractivity and related propagation effects are of main interest. The statistical data important for the design of terrestrial radio systems have to be obtained from the experiments, an example of which is described further.

3. Measurement of refractivity and propagation

3.1 Measurement setup

A propagation experiment focussed on the atmospheric refractivity related effects has been carried out in the Czech Republic since November 2007. First, the combined experiment consists of the measurement of a received power level fluctuations on the microwave terrestrial path operating in the 10.7 GHz band with 5 receiving antennas located in different heights above the ground. Second, atmospheric refractivity is determined in the several heights (19 heights from May, 2010) at the receiver site from pressure, temperature and relative humidity that are simultaneously measured by a meteo-sensors located on the 150 meters tall mast. Refractivity is calculated using (2) – (4). Figure 2a shows the terrain profile of the microwave path.
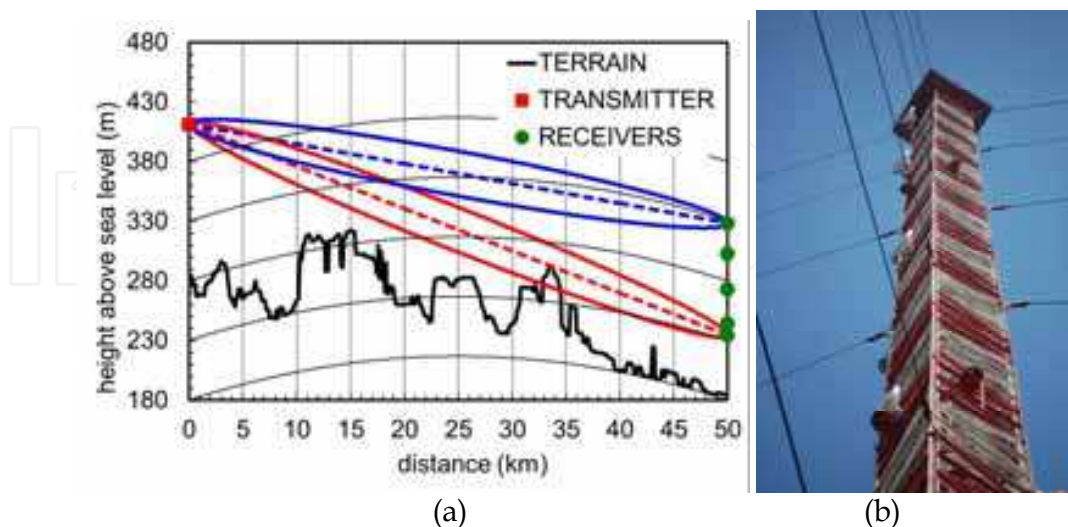

Fig. 2. (a) The terrain profile of an experimental microwave path, TV Tower Prague – Podebrady mast, with the first Fresnel ellipsoids of the lowest and the highest paths for $k = R_{ef}/R = 4/3$, (b) the parabolic receiver antennas placed on the 150 m high mast (Podebrady site).

The distance between the transmitter and receivers is 49.8 km. It can be seen in Fig. 2a a terrain obstacle located about 33 km from the transmitter site. The height of the obstacle is such that about 0% of the first Fresnel ellipsoid radius of the lowest path (between the transmitter antenna and the lowest receiver antenna) is free. It follows that under standard atmospheric conditions ($k = R_{ef}/R = 4/3$) the lowest path is attenuated due to the diffraction loss of about 6 dB. Tables 1a and 1b show the parameters of the measurement setup.

Heights of meteorological sensors	5.1 m, 27.6 m, 50.3 m, 75.9 m, 98.3 m, 123.9 m, 19 sensors approx. every 7 m (from May 2010)
Pressure sensor height	1.4 m
Temperature/humidity sensor	Vaisala HMP45D, accuracy ±0.2°C, ±2% rel. hum.
Pressure sensor	Vaisala PTB100A, accuracy ±0.2 hPa

Table 1a. The parameters of a measurement system (meteorology).

TX tower ground altitude	258.4 m above sea level
TX antenna height	126.3 m
Frequency	10.671 GHz
Polarization	Horizontal
TX output power	20.0 dBm
Path length	49.82 km
Parabolic antennas	diameter 0.65 m, gain 33.6 dBi
RX dynamical range	> 40 dB
RX tower ground altitude	188.0 m above sea level
RX antennas heights	51.5 m, 61.1 m, 90.0 m, 119.9 m, 145.5 m
Est. uncertainty of received level	±1 dB

Table 1b. The parameters of a measurement system (radio, TX = transmitter, RX = receiver).

3.2 Examples of refractivity effects

In order to get a better insight into atmospheric refractivity impairments occurring in real atmosphere, several examples of measured vertical profiles of temperature, relative humidity, modified refractivity and of received signal levels are given. The modified refractivity M is calculated from refractivity N as:

$$M(h) = N(h) + 157h \qquad (7)$$

where h(km) stands for the height above the ground. The reason of using M instead of N here is to clearly point out the possible ducting conditions ($dN/dh < -157$ N-units/km) when $dM/dh < 0$ M-units/km.

Figure 3 shows the example of radio-meteorological data obtained during a very calm day in autumn 2010. The relative received signal levels measured at 51.5 m (floor 0), 90.0 m (floor 2) and at 145.5 m (floor 4) are depicted. The lowest path (floor 0) is attenuated of about 6 dB due to diffraction on a path obstacle. The situation is atypical since the received signal level is very steady and does not fluctuate practically. The vertical gradient of modified refractivity has approximately the same value ($\approx$ 110 M-units/km or -47 N-units/km) during the whole day, the propagation conditions correspond to standard atmosphere.

A more typical example of measured data is shown in Fig. 4. Temperature and relative humidity change appreciably with height and in time. Specifically, temperature inversion is seen before 4:00 and after 20:00, the standard gradient takes place in the middle of the day. The received signal level recorded on the lowest path shows a typical enhancement at the beginning and at the end of the day which is caused by super-refractive propagation conditions. On the other hand the signal received at the higher antennas fluctuates mildly around 0 dB with more pronounced variations of the signal in the morning and at night.

Sub-refractive propagation conditions were observed between 2:00 and 4:00 on 14 October 2010 as shown in Fig. 5. One can see that increased attenuation due to diffraction on the path obstacle appears on the lowest path (floor 0) at that time. This well corresponds with the sub-refractive gradient of modified refractivity observed; see the lower value of dM/dh near the ground between 2:00 and 4:00 which is caused by strong temperature inversion together with no compensating humidity effect. The received signal measured on the higher antennas that are not affected by diffraction stays around the nominal value with some smaller fluctuations probably due to multipath and focusing/defocusing effects.

A typical example of multipath propagation is shown in Fig. 6. In the middle of the day from about 7:00 to 18:00, the received signal is steady at all heights and the atmosphere seems to be well mixed. On the other hand, multipath propagation occurring in the morning and at night is characterized by relatively fast fluctuations of the received signal. It is seen that all the receivers are impaired in the particular multipath events. Deep fading (attenuation > 20 dB) is quite regularly changing place with significant enhancement of the received signal level.
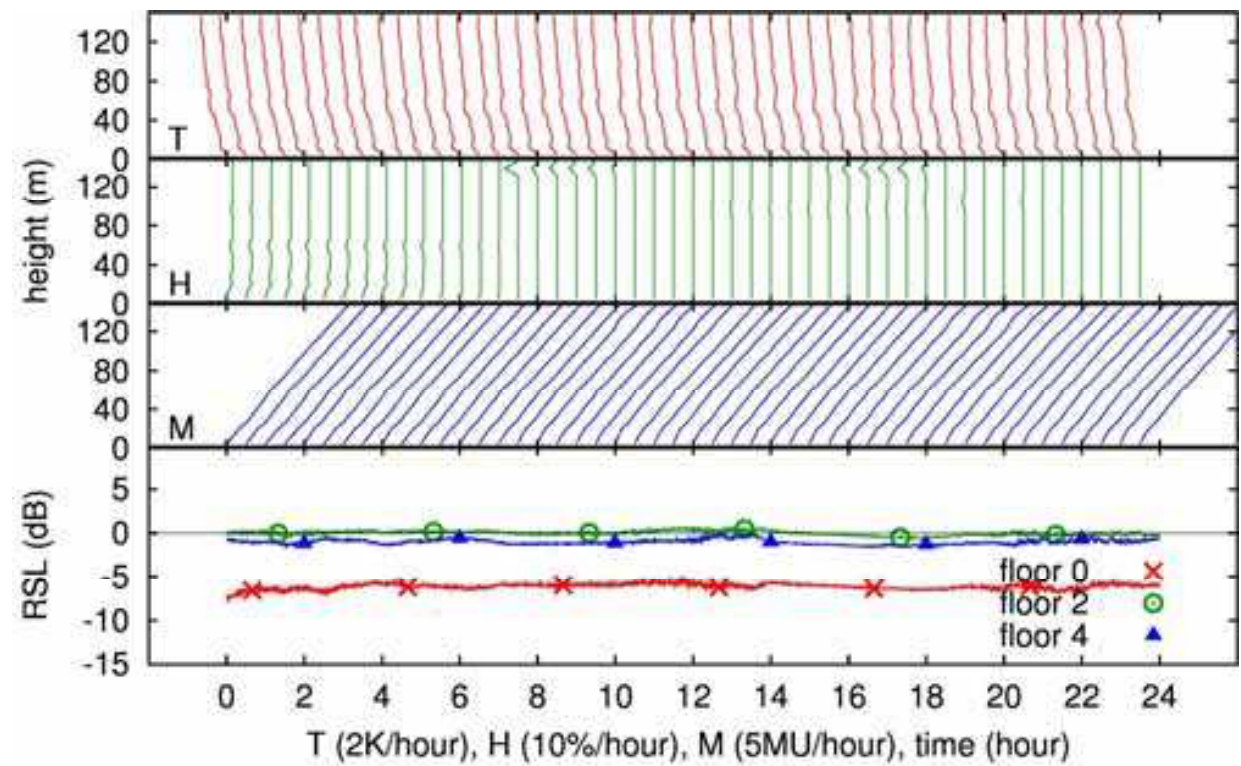

Fig. 3. The vertical profiles of temperature T, relative humidity H, modified refractivity M and received signal levels relative to free-space level observed on 17 November 2010
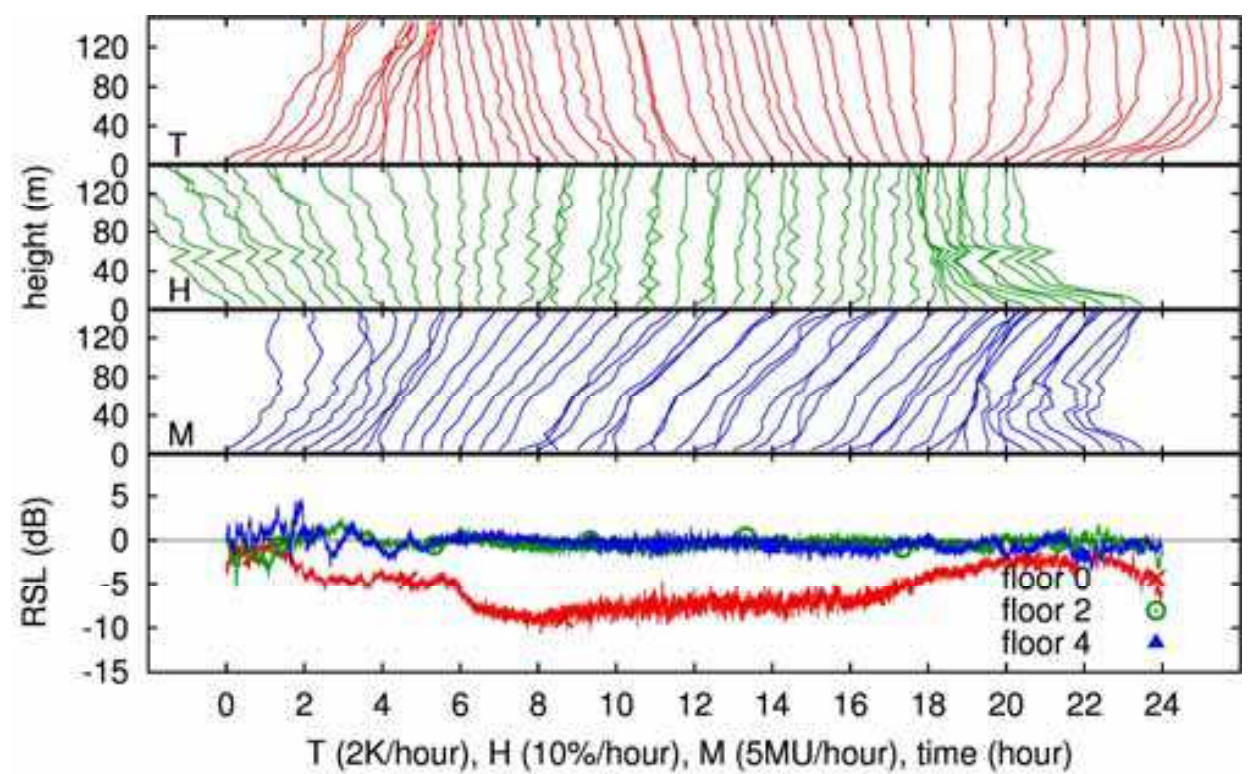
Fig. 4. The vertical profiles of temperature *T*, relative humidity *H*, modified refractivity *M* and received signal levels relative to free-space level observed on 26 June 2010
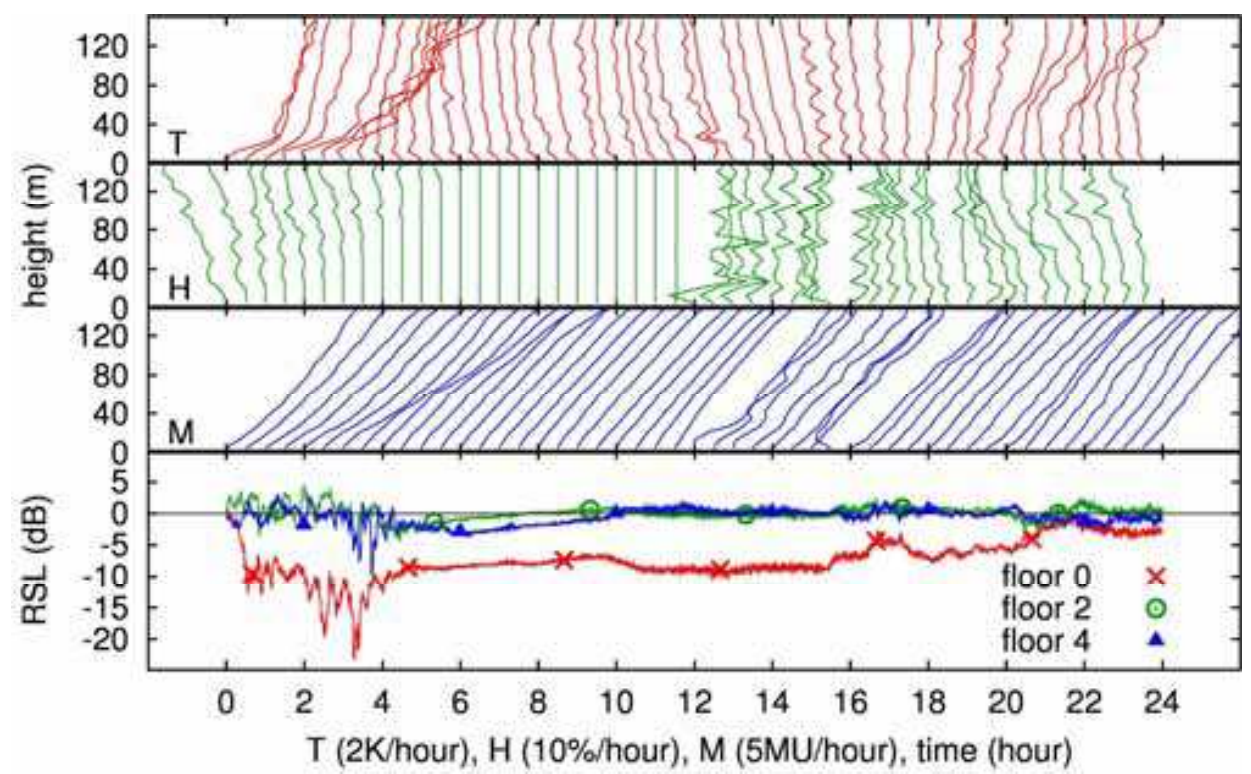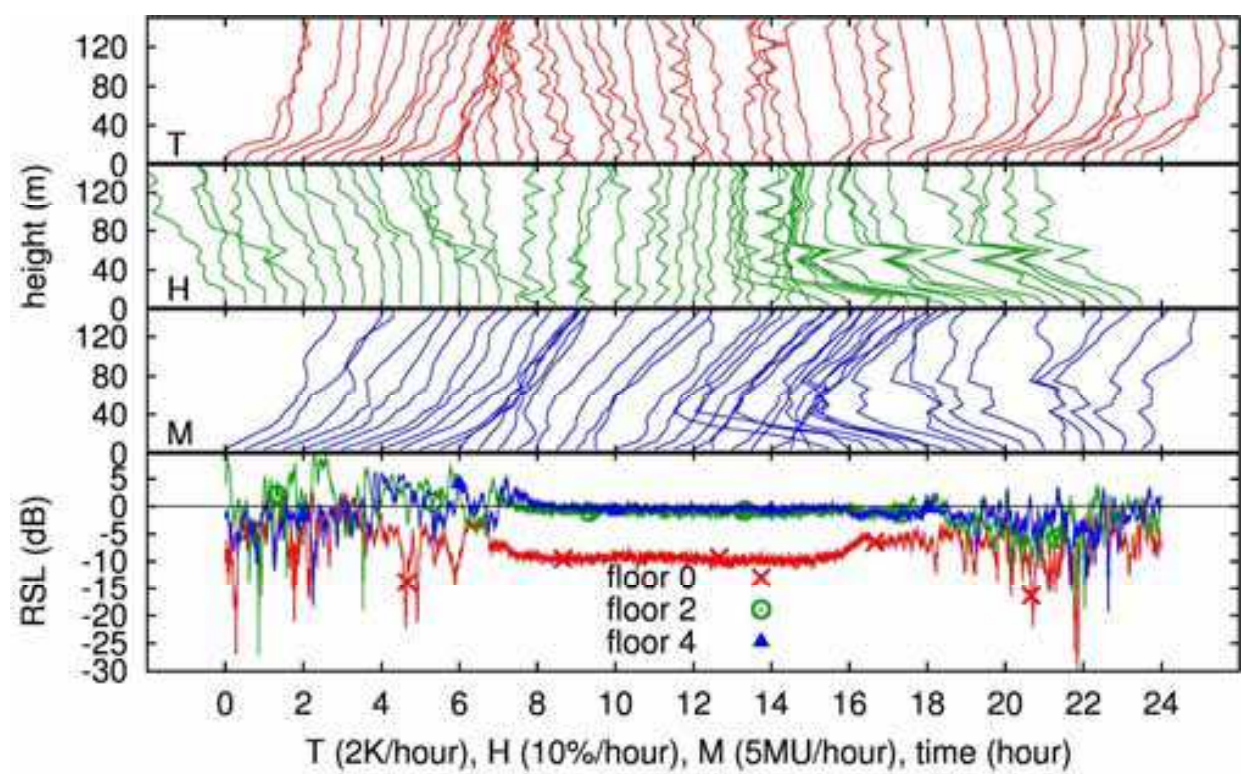

Fig. 5. The vertical profiles of temperature *T*, relative humidity *H*, modified refractivity *M* and received signal levels relative to free-space level observed on 14 October 2010

Fig. 6. The vertical profiles of temperature *T*, relative humidity *H*, modified refractivity *M* and received signal levels relative to free-space level observed on 12 September 2010

4. Refractivity statistics

As already mentioned, the physical processes in troposphere are complex enough to allow only statistical description of spatial and temporal characteristics of atmospheric refractivity. Nevertheless the statistics of important refractivity parameters such as an average vertical gradient are extremely useful in practical design of terrestrial radio paths when the long term statistics of the received signal have to be estimated, see (Rec. ITU-R P.530-12, 2009).

4.1 Average vertical gradient of refractivity

The prevailing vertical gradient of refractivity can be regarded as the single most important characteristics of atmospheric refractivity. According to (6), it is related to the effective Earth radius discussed above and it specifically determines the influence of terrain obstacles on terrestrial radio propagation paths. The examples of measured vertical profiles presented in the previous section show that the near-ground refractivity profile evolution is complex enough to not be described by only a single value of the gradient. The question arises what should be considered as a prevailing vertical gradient at a particular time. The gradient value is usually obtained from the refractivity difference at fixed heights, e.g. at 0 and 65 meters above the ground (Rec. ITU-R P.453-9, 2009). If more accurate data is available, the prevailing vertical gradient of refractivity can be calculated using a linear regression approach.

Two year data (2008-2009) of measured vertical profiles were analysed by means of linear regression of refractivity in the heights (0 – 120 m) and the statistics of the vertical gradient so obtained were calculated. The results are in Fig. 7a where the annual cumulative distribution functions of the gradient are depicted. The quantiles provided by ITU-R

datasets are also shown for comparison. It is clear that extreme gradients are less probable in reality than predicted by ITU-R. Linear regression tends to filter out the extreme gradients (otherwise obtained from two-point measurements) which do not fully represent the vertical distribution as a whole.
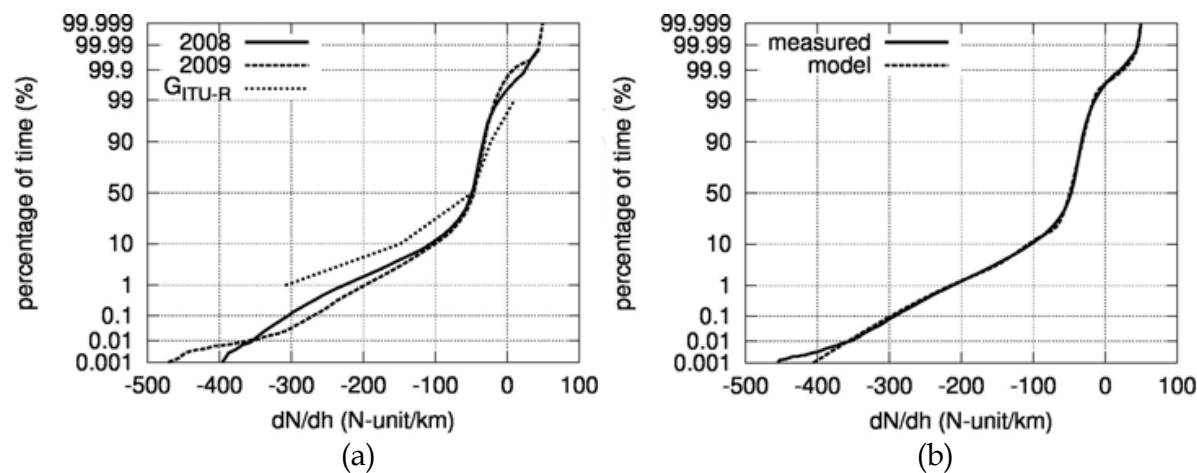

(a) (b)

Fig. 7. Annual cumulative distributions of the vertical gradient of atmospheric refractivity obtained in 2008, 2009 (a), cumulative distribution obtained from the whole season (2 years) and fitted model (b).

Taking into account the importance of the gradient statistics for the design of terrestrial radio path, it seems desirable to have a suitable model. Several models of the gradient statistics were proposed, see (Brussaard, 1996), that can be fitted to measured data. Since they are often discontinuous in the probability density, they can be thought to be little unnatural. One can see in Fig. 7b where the two-year cumulative distribution is shown that the distribution consists of three parts: the part around the standard (median) gradient and two other parts – tails. Therefore the following model of the probability density $f(x)$ and of the cumulative distribution function $F(x)$ is proposed:

$$f(x) = \sum_{i=1}^{3} p_i \frac{1}{\sigma\sqrt{2\pi}} \exp\left[\frac{(x-\mu_i)^2}{2\sigma_i^2} \right]; \qquad \sum_{i=1}^{3} p_i = 1 \qquad (8)$$

$$F(x) = \sum_{i=1}^{3} p_i \frac{1}{2}\left[1 + \mathrm{erf}\left(\frac{x-\mu_i}{\sigma_i\sqrt{2}} \right) \right] \qquad (9)$$

where the p_i, μ_i and σ_i are the relative probabilities, the mean values and the standard deviations of the Gaussian distributions forming the three parts of the whole distribution. Fitted model parameters (see Fig. 7b) are summarized in Table 2.

i	p_i	μ_i	σ_i
1	0.086	–128.0	75.1
2	0.793	–46.1	11.8
3	0.121	–99.6	24.8

Table 2. Vertical refractivity gradient distribution parameters

4.2 Ducting layers

Although the ducting layers appearing in the first several tens or hundreds meters above the ground have significant impact on the propagation of EM waves on nearly horizontal paths, surprisingly little is known about their occurrence probabilities or about their spatial/temporal properties (Ikegami et al., 1966). This is true especially in the lowest troposphere where the usual radio-sounding data suffers from insufficient spatial and also time resolution. In the following, the parameters of ducting layers observed during the experiment are analysed by means of the modified Webster duct model.

An analytic approach to the modelling of refractivity profiles was proposed in (Webster, 1982). The refractivity profile with the height h (m) was to be approximated by the formula similar to the following modified model:

$$N(h) = N_0 + G_N h + \frac{dN}{2} \tanh \frac{2.96(h - h_0)}{dh} \qquad (10)$$

where the refractivity N_0 (N-units), the gradient G_N (N-units/m), the duct depth dN (N-units), the duct height h_0 (m) and the duct width dh (m) are model parameters. A hyperbolic tangent is used in (10) instead of arctangent in the original Webster model because the "tanh" function converges faster to a constant value for increasing arguments than the "arctan" does. As a consequence, there is a sharper transition between the layer and the ambient gradient in the modified model and so the duct width values dh are more clearly recognizable in profiles. Figure 8 shows the meaning of the model parameters by an example where the modified refractivity profile is also included. It is seen from (7) and (10) that the model for modified refractivity profiles differs only in the value of the gradient: $G = G_N + 0.157$ (N-units/m).
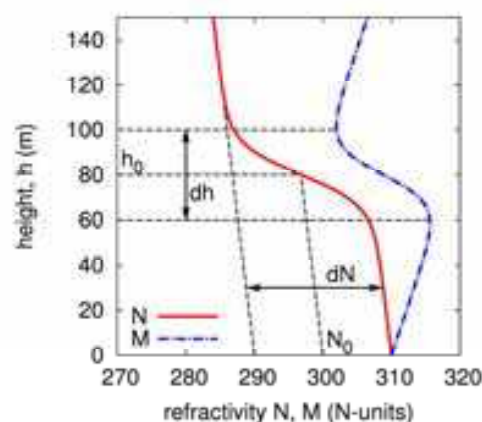

Fig. 8. Duct model parameter definition with the values of parameters: N_0 = 300 N-units, G_N = -40 N-units/km, dN = -20 N-units, h_0 = 80 m, dh = 40 m.

The above model was fitted to the refractivity profiles measured in between May and November 2010. More than $3 \cdot 10^5$ profiles were analysed and related model parameters were obtained. Figure 9 shows two examples of 1-hour measured data and fitted models. Significant dynamics is clearly seen in the evolving elevated ducting layers. It is also clear from the examples in Fig. 9 that the model is not able to capture all the fine details of measured profiles but it serves very well to describe the most important features relevant for radio propagation studies. Sometimes, the part or the whole ducting layer is located

above the measurement range and so it is out of reach of modelling despite its effect on the propagation might be serious. This should be kept in mind while studying the statistical results presented below.

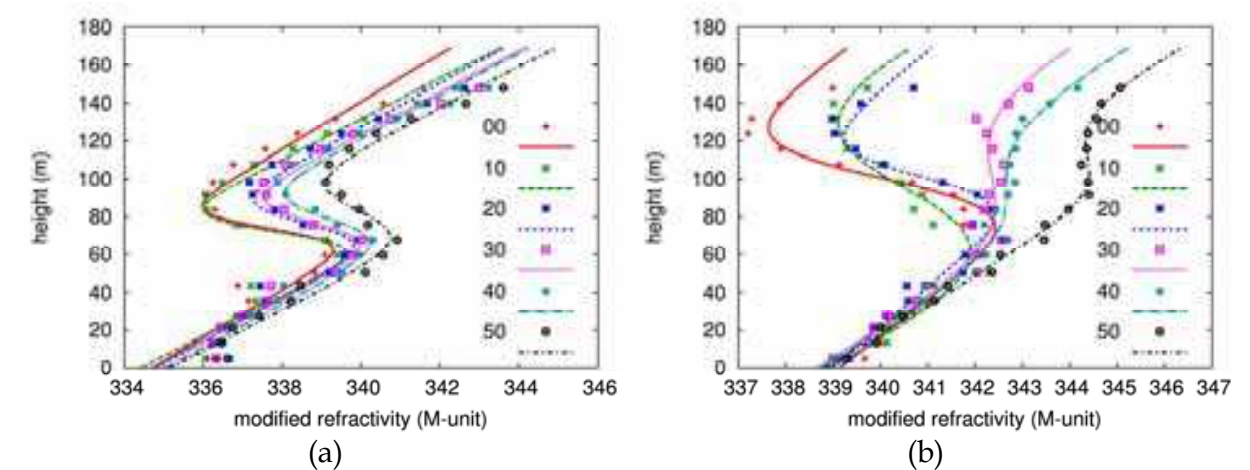(a)   (b)

Fig. 9. The examples of time evolution of elevated ducting layers observed on the 1st of August 2010 at 00:00-00:50 (a) and on the 14th of July 2010 at 22:00-22:50 (b), measured data with points, fitted profiles with lines.

Figure 10 shows the empirical cumulative distributions of duct model parameters obtained from the fitting procedure. The medians (50% of time) of duct parameters can be read as $N_0 = 320$ N-units, $G = 116$ N-units/km, $dN = -2.2$ N-units, $h_0 = 61$ m, $dh = 73$ m. The probability distributions of N_0 and G are almost symmetric around the median. On the other hand, the depth dN and width dh distributions are clearly asymmetric showing that the smaller negative values of the depth and the smaller values of width are observed more frequently. Almost linear cumulative distribution of the duct height h_0 between 50 and 100 m above the ground suggests that there is no preferred duct height here.
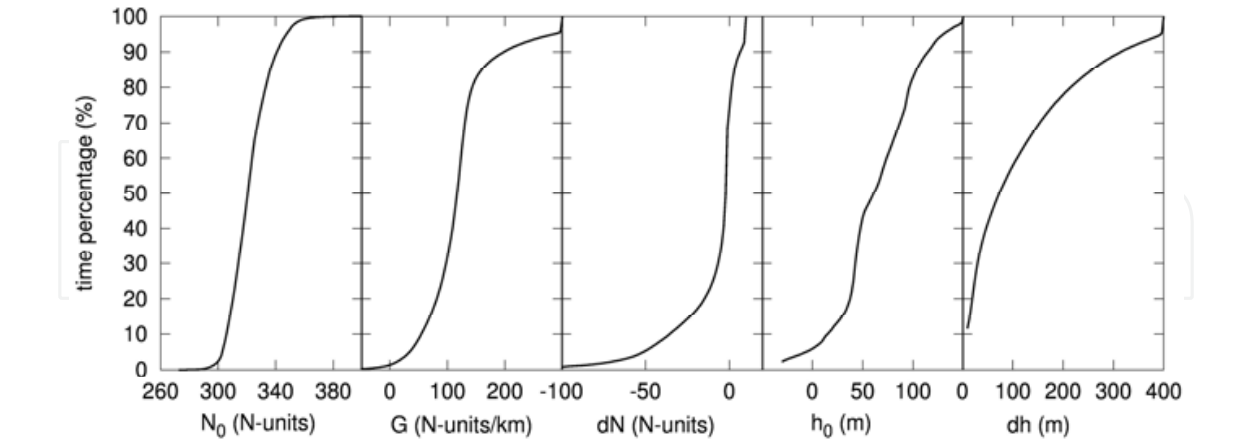

Fig. 10. The cumulative distribution functions of duct parameters obtained from measured profiles of atmospheric refractivity at Podebrady, 05/2010 – 11/2010.

Important interrelations between duct parameters are revealed by empirical joint probability density functions (PDF) presented in Fig. 11 – 15. The 2D maps show the logarithm of joint PDFs of all combinations of 5 parameters of the duct model (10). In these plots, dark areas mean the high probability values and light areas mean the low probability values. It is

generally observed that there are certain preferred areas in the parameter space where the combinations of duct parameters usually fall in. For example, it is seen in Fig. 13a that the absolute value of the negative duct depth is likely to increase with the increasing gradient G. On the other hand, there are empty areas in the parameter space where the combinations of parameters are not likely to appear. One may find this information helpful when analysing terrestrial propagation using random ducts generated by the Monte Carlo method.

(a)   (b)
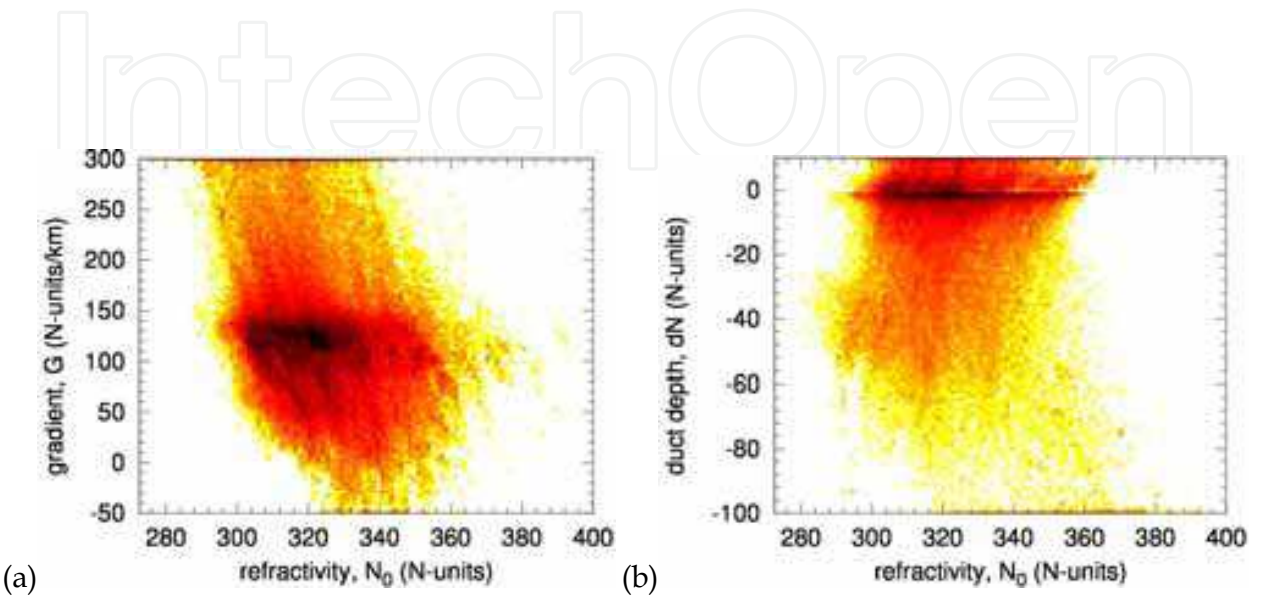
Fig. 11. The logarithm of the joint probability density function of duct parameters, obtained from measured profiles of atmospheric refractivity at Podebrady, 05/2010 – 11/2010.
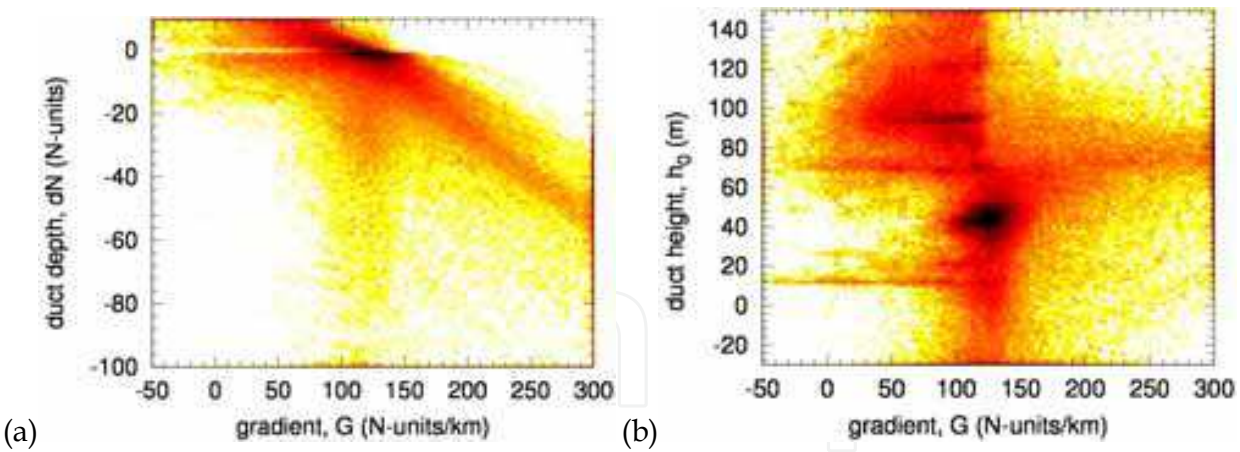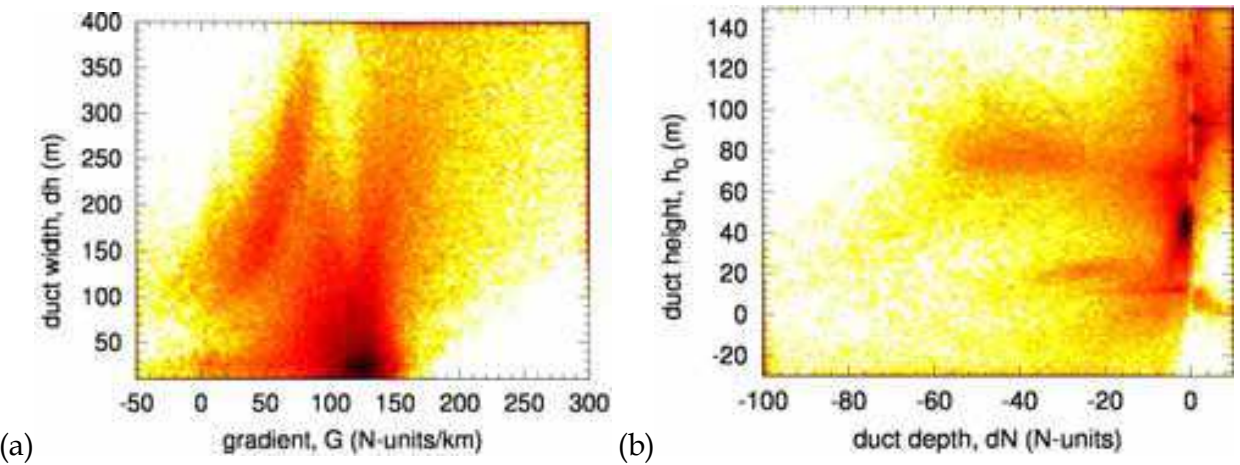

(a)   (b)
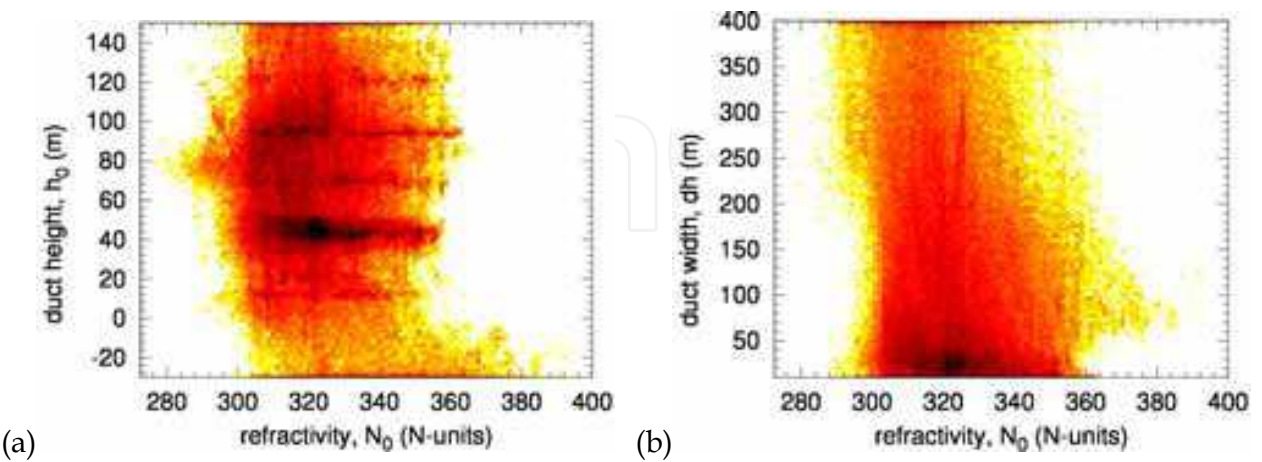
Fig. 12. The logarithm of the joint probability density function of duct parameters, obtained from measured profiles of atmospheric refractivity at Podebrady, 05/2010 – 11/2010.
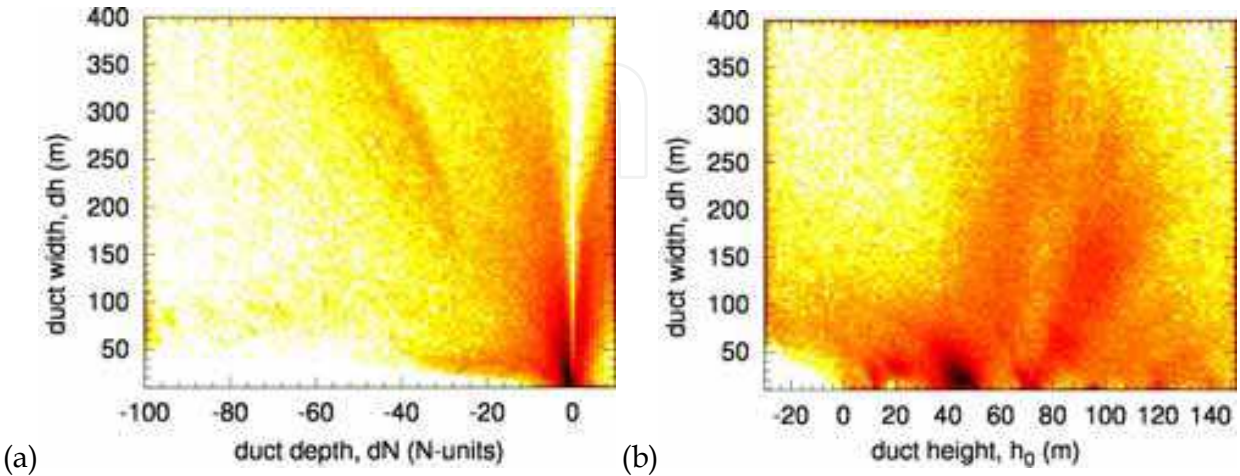
Fig. 13. The logarithm of the joint probability density function of duct parameters, obtained from measured profiles of atmospheric refractivity at Podebrady, 05/2010 – 11/2010.

Fig. 14. The logarithm of the joint probability density function of duct parameters, obtained from measured profiles of atmospheric refractivity at Podebrady, 05/2010 – 11/2010.

Fig. 15. The logarithm of the joint probability density function of duct parameters, obtained from measured profiles of atmospheric refractivity at Podebrady, 05/2010 – 11/2010.

5. Modelling of EM waves in the troposphere

Several numerical methods have been used in order to assess the effects of atmospheric refractivity on the propagation of electromagnetic waves in the troposphere. They can be roughly divided into two categories - ray tracing methods based on geometrical optics and full-wave methods. The ray tracing methods numerically solve the ray equation (5) in order to get the ray trajectories of the electromagnetic wave within inhomogeneous refractivity medium. The ray tracing provides a useful qualitative insight into refraction phenomena such as bending of electromagnetic waves. Its utilization for quantitative modelling is limited to conditions where the electromagnetic waves of sufficiently large frequency may be approximated by rays. Geometrical optics description is known to fail at focal points and caustics where the full-wave methods provide more accurate results.

The full-wave numerical methods solve the wave equation that is a partial differential equation. Among time domain techniques, finite difference time domain (FDTD) based approaches were proposed (Akleman & Sevgi, 2000) that implement sliding rectangular window where 2D FDTD algorithm is applied. Nevertheless, tropospheric propagation simulation in frequency domain is more often. In particular , there is a computationally efficient approach based on the paraxial approximation of Helmholtz wave equation, so called Parabolic Equation Method (PEM), which is the most often used full-wave method in tropospheric propagation.

5.1 Split step parabolic equation method

We start the brief summary of PEM (Levy, 2000) with the scalar wave equation for an electric or magnetic field component ψ:

$$\nabla^2\psi + k^2 n^2 \psi = 0 \tag{11}$$

where $k = 2\pi/\lambda$ is the wave number in the vacuum and $n(r,\theta,\varphi)$ is the refractive index. Spherical coordinates with the origin at the center of the Earth are used here. Further, we assume the azimuthal symmetry of the field, $\psi(r,\theta,\varphi) = \psi(r,\theta)$, and express the wave equation in cylindrical coordinates:

$$\frac{\partial^2\psi}{\partial z^2} + \frac{\partial^2\psi}{\partial x^2} + \frac{1}{x}\frac{\partial\psi}{\partial x} + k^2 m^2(x,z)\psi = 0 \tag{12}$$

where:

$$m(x,z) = n(x,z) + z/R \tag{13}$$

is the modified refractive index which takes account of the Earth's radius R and where $x = r\theta$ is a horizontal range and $z = r - R$ refers to an altitude over the Earth's surface. We are interested in the variations of the field on scales larger than a wavelength. For near horizontal propagation we can separate "phase" and "amplitude" functions by the substitution of:

$$\psi(x,z) = u(x,z)\frac{e^{jkx}}{\sqrt{x}} \tag{14}$$

in equation (12) to obtain:

$$\frac{\partial^2 u}{\partial z^2} + \frac{\partial^2 u}{\partial x^2} + 2jk\frac{\partial u}{\partial x} + k^2\left(m^2 - 1 + \frac{1}{(2kx)^2}\right)u = 0 \tag{15}$$

Paraxial approximation is made now. The field $u(x,z)$ depends only little on z, because main dependence of $\psi(x,z)$ is covered in the $\exp(jkx)$ factor in (14). Then it is assumed that:

$$\left|\frac{\partial^2 u}{\partial x^2}\right| << 2k\left|\frac{\partial u}{\partial x}\right| \tag{16}$$

and the $1/(2kx)^2$ term can be removed from (15) since $kx >> 1$ when the field is calculated far enough from a source. We obtain the following parabolic equation:

$$\frac{\partial^2 u}{\partial z^2} + 2jk\frac{\partial u}{\partial x} + k^2(m^2(x,z) - 1)u = 0 \tag{17}$$

An elliptic wave equation is therefore simplified to a parabolic equation where near horizontal propagation is assumed. This equation can be solved by the efficient iterative methods such as the Fourier split-step method. Let us assume the modified refractivity m is constant. Then we can apply Fourier transform on the equation (17) to get:

$$-p^2 U + 2jk\frac{\partial U}{\partial x} + k^2(m^2 - 1)U = 0 \tag{18}$$

where Fourier transform is defined as:

$$U \equiv U(x,p) = \mathrm{F}\{u(x,z)\} = \int_{-\infty}^{\infty} u(x,z)e^{-jpz}\mathrm{d}z \tag{19}$$

From (18), we obtain:

$$\frac{\partial U(x,p)}{\partial x} = \left(\frac{p^2 - k^2(m^2 - 1)}{2jk}\right)U(x,p) \tag{20}$$

$$U(x,p) = e^{-jx(p^2/(2k))} \cdot e^{jx(k(m^2-1)/2)} \tag{21}$$

and we get the formula for step-by-step solution:

$$U(x + \Delta x, p) = \left(e^{-j\Delta x(p^2/(2k))} \cdot e^{j\Delta x(k(m^2-1)/2)}\right)U(x,p) \tag{22}$$

The field in the next layer $u(x+\Delta x,z)$ is computed using the field in the previous layer $u(x,z)$:

$$u(x + \Delta x, z) = e^{j\Delta x(k(m^2-1)/2)} \cdot \mathrm{F}^{-1}\left\{U(x,p)e^{-j\Delta x(p^2/(2k))}\right\} \tag{23}$$

Fourier transformation is applied in z-direction and the variable p represents the "spatial frequency" (wave number) of this direction: $p = k_z = k\sin(\xi)$ and ξ is the angle of propagation.

The assumption that *m* is constant is not fulfilled, but equation (23) is used anyway. The resulting error is proportional to Δx and to horizontal and vertical gradients of refractivity. In practice, the value of Δx can be of several hundred wavelengths.

5.2 Application example and comparison with measured data

The parabolic equation method outlined above has been applied frequently to investigate the propagation characteristics on terrestrial (and also on Earth - space) paths under the influence of different refractivity conditions (Barrios, 1992, 1994; Levy, 2000) including the ducting layers described in the section 4.2. Users agree the method gives reliable results provided all the relevant details of terrain profile and of refractivity distribution are known and modelled correctly. This is however not always the case in practice. It is believed that the modelling results have to be compared with real world data whenever possible in order to validate the method under different propagation conditions and to know more about the expected errors due to incomplete knowledge of propagation medium.

Let us illustrate the particular example of conditions where the parabolic equation method performs successfully regardless the fact that refractivity profile along the propagation path is only roughly estimated. Figures 16a and 16b show the results of PEM propagation simulation performed using refractivity gradients measured during the 4th of November, 2008 at the receiver site. Sub-refractive conditions that occurred early morning caused a significant diffraction fading of more than 20 dB on the two lowest paths see Fig. 16b. On the other hand, the higher paths (receiving antennas located at 90 m and above) were not affected by diffraction effects.
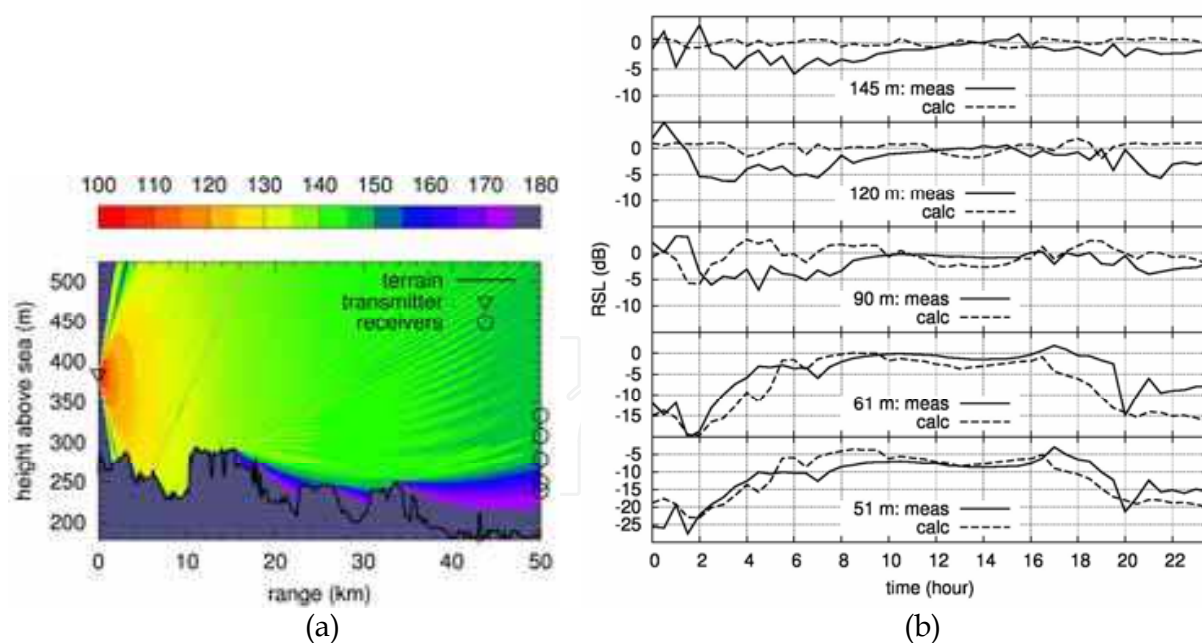

Fig. 16. Spatial distribution of received power loss during sub-refractive condition on the path TV Tower Prague – Podebrady calculated by PEM (a), received signal levels measured in 5 receivers located in different heights and received signal levels modelled by PEM using time dependent vertical gradient of refractivity (b).

The results shown in Fig. 16b confirm that a very good agreement between PEM simulation and measurement can be achieved if the diffraction fading due to sub-refractive conditions

(see time about 2:00) is the most important effect influencing the received power. It suggests that sub-refractive gradients are likely to be approximately the same along the whole propagation path and the approximation of horizontally independent refractivity, which is usually applied in PEM, is reasonable in this case. On the other hand, similar conclusion cannot be reached when multipath propagation occurs because only slight change in a refractivity profile along the propagation path may vary the received power distribution profoundly. These facts have to be kept in mind when the simulation results are interpreted.

6. Conclusion

Some results of the ongoing studies focussed on the propagation impairments of the atmospheric refractivity in the lowest troposphere were presented. Concurrent measurements of the vertical distribution of atmospheric refractivity together with the multi-receiver microwave propagation experiment were described. A new statistical model of vertical refractivity gradient was introduced. The unique joint statistics of ducting layers parameters were presented. The application of parabolic equation method was demonstrated on the example of a diffraction fading event. Simulated and measured time series were compared. A good agreement between simulation and measured data has been witnessed.

Future works in the area of the atmospheric refractivity related propagation effects should, for example, investigate the relations between the time evolution of duct parameters and multipath propagation characteristics, which is the area where only little is known at this moment.

7. Acknowledgment

8. References

Akleman, F.; Sevgi, L. (2000). A novel time-domain wave propagator. *IEEE Transactions on Antennas and Propagation,* Vol. 48, No. 5, (May 2000), pp. (839-841), 0018-926X

Barrios, A. (1992). Parabolic equation modelling in horizontally inhomogeneous environments. *IEEE Transactions on Antennas and Propagation,* Vol. 40, No. 7, (July 1992), pp. (791-797), 0018-926X

Barrios, A. (1994). A terrain parabolic equation model for propagation in the troposphere. *IEEE Transactions on Antennas and Propagation,* Vol. 42, No. 1, (January 1994), pp. (90-98), 0018-926X

Brussaard, G. (Ed.). (1996). *Handbook on Radiometeorology,* International Telecommunication Union, ISBN 92-61-06241-5, Geneva, Switzerland.

Ikegami, F.; Haga, M.; Fukuda, T.; Yoshida, H. (1966). Experimental studies on atmospheric ducts and microwave fading. *Review of the Electrical Communication Laboratory,* Vol. 14, No. 7-8, (July-August 1966), pp. (505-533)

Kerr, D. E. (Ed.). (1987). *Propagation of Short Radio Waves,* Peter Peregrinus Ltd./IEE, ISBN 0-86341-099-5, London, UK.

Lavergnat, J.; Sylvain, M. (2000). *Radio Wave Propagation: Principles and Techniques,* John Wiley & Sons., ISBN 0-471-49027-X, Chichester, UK.

Levy, M. (2000). *Parabolic Equation Methods for Electromagnetic Wave Propagation,* The Institution of Electrical Engineers, ISBN 0-85296-764-0, London, UK.

Rec. ITU-R P.453-9 (2009). The radio refractive index: its formula and refractivity data, *ITU-R Recommendations and Reports*, ITU, Geneva, Switzerland, 2009.

Rec. ITU-R P.530-12 (2009). Propagation data and prediction methods required for the design of terrestrial line-of-sight systems, *ITU-R Recommendations and Reports*, ITU, Geneva, Switzerland, 2009.

Webster, A. R. (1982). Raypath parameters in tropospheric multipath propagation. *IEEE Transactions on Antennas and Propagation,* Vol. 30, No. 4, (July 1982), pp. (796-800), 0018-926X
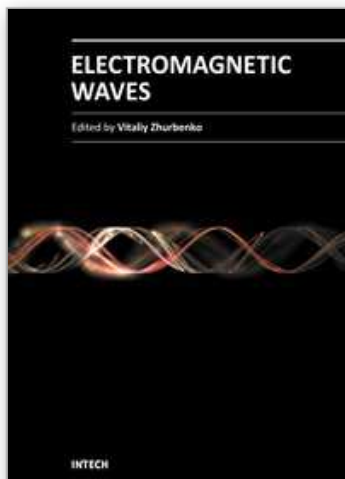
Electromagnetic Waves

Edited by Prof. Vitaliy Zhurbenko

This book is dedicated to various aspects of electromagnetic wave theory and its applications in science and technology. The covered topics include the fundamental physics of electromagnetic waves, theory of electromagnetic wave propagation and scattering, methods of computational analysis, material characterization, electromagnetic properties of plasma, analysis and applications of periodic structures and waveguide components, and finally, the biological effects and medical applications of electromagnetic fields.

How to reference

In order to correctly reference this scholarly work, feel free to copy and paste the following:

Martin Grabner and Vaclav Kvicera (2011). Atmospheric Refraction and Propagation in Lower Troposphere, Electromagnetic Waves, Prof. Vitaliy Zhurbenko (Ed.), ISBN: 978-953-307-304-0, InTech, Available from: http://www.intechopen.com/books/electromagnetic-waves/atmospheric-refraction-and-propagation-in-lower-troposphere

INTECH
open science | open minds